Mineralium Deposita (2024) 59:155–167
https://doi.org/10.1007/s00126-023-01201-y

ARTICLE

Inverse Mo versus U isotope correlation of Early Cambrian highly metalliferous black shales in South China indicates synsedimentary metal enrichment from a near-modern ocean

Lingang Xu[1,2] · Bernd Lehmann[3] · Stefan Weyer[4] · Hanjie Wen[5] · Jingwen Mao[1,2] · Nadia Neubert[4] · Wei Jian[1,2]

Received: 15 July 2022 / Accepted: 2 August 2023 / Published online: 18 August 2023

Abstract

The basal unit of the Early Cambrian black shale sequence of South China hosts sulfide-rich polymetallic units, non-sulfidic vanadium-rich black shales, sapropelic alginite (combustible shale), barite, and phosphorite. This rock spectrum occurs in a paleoceanographic similar, and stratigraphically correlated, transgressive upwelling setting on the passive continental margin of the Neoproterozoic Yangtze Platform. Several centimeter-thick polymetallic sulfidic units (3–13 wt% Mo+Ni, 100–600 ppm U) have relatively light Mo ($\delta^{98/95}$Mo = 1.1 ± 0.2‰) and relatively heavy U isotope composition ($\delta^{238/235}$U = 0.2 ± 0.1‰). Several meter-thick V-rich shales with multiple ore-grade layers (0.1–0.8 wt% V, < 100 ppm U, Mo and Ni ~ 100 ppm) have isotopically lighter Mo ($\delta^{98/95}$Mo = 0.3 ± 0.4‰) and heavier U composition ($\delta^{238/235}$U = 0.4 ± 0.2‰ and up to 0.7‰). The inverse Mo versus U isotope correlation suggests that both metals were enriched by removal from anoxic to strongly euxinic bottom water in restricted basins along the rifted continental margin. Metal replenishment probably occurred via the cycling of Fe–Mn-oxyhydroxide particles across the redox boundary, with sorption/desorption of Mo (and likely Ni) in a stratified water column. In contrast, V enrichment with much lower Mo, Ni, and U contents, but more fractionated Mo and U isotope composition, reflects non-sulfidic anoxic depositional conditions in a partly open system with higher bottom water renewal rates. While Mo isotope fractionation likely occurred in the water column, U isotope fractionation may dominantly have occurred at the water-sediment interface, perhaps in a benthic organic flocculent layer. These findings indicate that local hydrodynamic control and stratified water column redox conditions may explain the observed variation of metal enrichment (Mo–Ni versus V) in the black shales. Furthermore, the high $\delta^{98/95}$Mo values up to 2.6‰ of the black shales studied and the correlated U and Mo isotope data suggest that Early Cambrian seawater was at least episodically broadly similar to modern seawater.

Keywords Mo isotopes · U isotopes · Ni–Mo-rich black shales · V-rich black shales · Early Cambrian · South China

Editorial handling: F. Melcher

✉ Lingang Xu
xulingang@cugb.edu.cn

1 School of Earth Sciences and Resources, China University of Geosciences, Beijing 100083, China

2 Key Laboratory for Exploration Theory & Technology of Critical Mineral Resources, Ministry of Natural Resources, Beijing 10083, China

3 Mineral Resources, Technical University of Clausthal, 38678 Clausthal-Zellerfeld, Germany

4 Institute of Mineralogy, Leibniz University Hannover, 30167 Hanover, Germany

5 State Key Laboratory of Ore Deposit Geochemistry, Institute of Geochemistry, Chinese Academy of Sciences, Guiyang 550002, China

Introduction

The Precambrian-Cambrian transition represents a dramatic change of the hydrosphere and biosphere in Earth history, with the Cambrian explosion of animal diversity which likely was linked to increased oxygen concentration in the oceans (Knoll and Carroll 1999; Sperling et al. 2013). However, the state of oxygenation of the oceans during the Early Cambrian is not well constrained and may have been variable (Kendall et al. 2015). Marine black shales provide a possibility to reconstruct local and global ocean redox conditions. These rocks commonly have elevated contents of authigenic redox-sensitive elements, which, together with their isotope compositions, document ancient seawater chemistry. For example, modern open oceans have homogeneous Mo

isotopic composition of $\delta^{98/95}$Mo ~ 2.3‰, due to the fact that deep-sea Fe–Mn sediments adsorb isotopically light Mo (Barling and Anbar 2004). Modern euxinic sediments (e.g., the Black Sea sapropels) with near-quantitative Mo capture display the open ocean Mo isotopic signal without isotope fractionation (Kendall et al. 2017). Therefore, Mo isotope compositions of euxinic sediments from the past may serve as proxies of paleoceanic redox conditions. Mo isotope data with high values of up to 2.5‰ $\delta^{98/95}$Mo for black shales and organic-rich cherts point to modern-like oxygenated seawater in the Early Cambrian (Chen et al. 2015; Wen et al. 2015; Cheng et al. 2020) and already in the Late Ediacaran (Kendall et al. 2015). This finding is in conflict with the interpretation of earlier Mo isotope data which suggested an overall much less oxygenated Early Cambrian Ocean with about 1.1 ± 0.1‰ $\delta^{98/95}$Mo, based on Mo isotope data from extremely sulfide- and metal-rich black shales (Lehmann et al. 2007; Wille et al. 2008; Xu et al. 2012, 2013). However, these lower values likely are due to the redox cycling of Mo via the "manganese and iron shuttle" (Scholz et al. 2013) which can generate Mo isotope signatures in between riverine input and seawater (see below).

The southeastern margin of the Late Neoproterozoic Yangtze carbonate-shale platform in South China is overlain by a transgressive sequence of Early Cambrian black shales (Niutitang Formation and equivalents) which in their basal part hosts synsedimentary polymetallic nickel-molybdenum, vanadium, phosphorite, barite, and sapropelic alginite (combustible shale/"stone coal") deposits (Fig. 1(a), Coveney Jr. et al. 1994; Mao et al. 2002; Xu et al. 2011, 2013; Lehmann

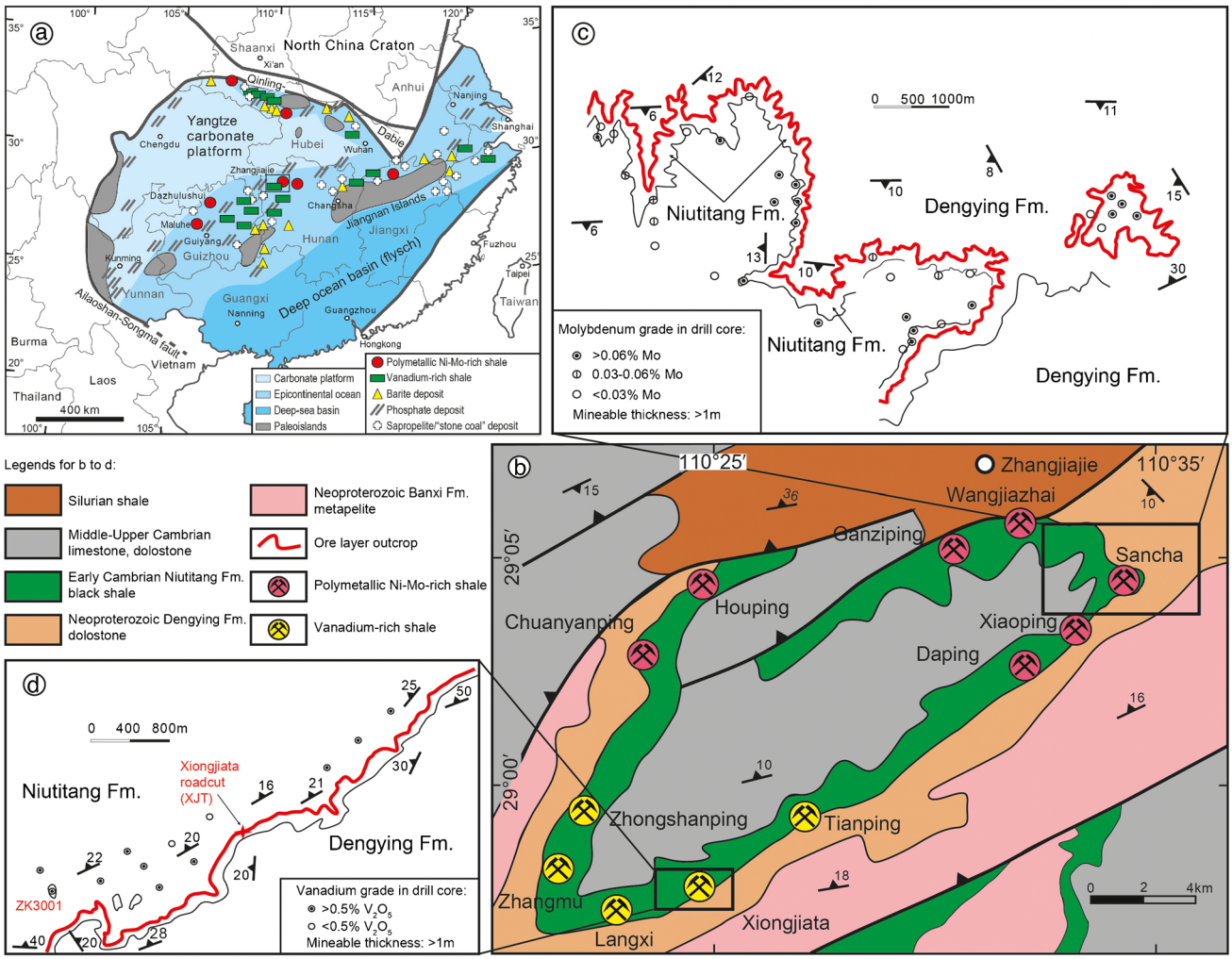

Fig. 1 (**a**) Early Cambrian paleogeographic situation of South China with black shale deposition on the margin of the rifted Yangtze Platform under conditions of high biological productivity in redox-stratified and sediment-starved marginal basins (modified from Lehmann et al. 2016). The metalliferous black shales are in the sediment-starved epicontinental ocean (light blue color), which is bordered by the Yangtze carbonate platform (very light blue) and the deep-sea basin (blue). The grey shaded areas are paleoislands. (**b**) Metallogenetic zonation of the polymetallic Ni–Mo-rich and V-rich black shales in the Zhangjiajie district. (**c**) Polymetallic Ni–Mo-rich shale in the Sancha mine. (**d**) Vanadium-rich shale in the Xiongjiata mine

et al. 2016, 2022; Yin et al. 2017). Paleogeographic and geochronological studies reveal that the polymetallic Ni–Mo-rich units and the V-rich shales are stratigraphically correlated (Xu et al. 2011; Xu and Mao 2021; Wu et al. 2021) but that the polymetallic Ni–Mo-rich unit dominantly occurs near the bottom of the sequence, whereas the V-rich shale can occur in several layers within a few tens of meters of stratigraphic thickness. Such a metal zonation pattern provides an opportunity to better understand the depositional heterogeneity of Early Cambrian marginal seas and, perhaps, a perspective on Cambrian paleo-seawater composition.

Molybdenum and uranium are highly redox-sensitive elements, and their isotopes are fractionated according to changes in seawater redox conditions (Andersen et al. 2017; Kendall et al. 2017). Mo is a conservative element with a long residence time of 760 kyr, which creates a homogeneous distribution of Mo in the ocean (Kendall et al. 2017). The Mo isotope composition of modern seawater is controlled by the preferential adsorption of isotopically light Mo to ferromanganese oxides and hydroxide phases in oxic sediments, resulting in Mo isotope fractionation of up to 2.7‰ in $\delta^{98/95}$Mo (Barling and Anbar 2004; Wasylenki et al. 2008; Goldberg et al. 2009). Under euxinic conditions, where dissolved $[H_2S]_{aq}$ exceeds a "switch point" at ~ 11 µM, dissolved molybdate (MoO_4^{2-}) is near quantitatively converted to highly particle-reactive tetra-thiomolybdate (MoS_4^{2-}), essentially without or only small isotopic fractionation (Barling et al. 2001; Tossell 2005; Neubert et al. 2008). The Mo isotope composition of marine sediments with near quantitative Mo uptake that formed under such reducing conditions, therefore, is close to coeval open ocean seawater (present-day seawater: $\delta^{98/95}Mo = 2.3 \pm 0.1$‰) (Kendall et al. 2017). Under weakly euxinic or suboxic conditions with $[H_2S]_{aq}$ below the switch point, only a fraction of molybdate is removed from seawater through thiomolybdate intermediate complexes ($MoO_xS_{4-x}^{2-}$), resulting in significantly lower and variable $\delta^{98/95}$Mo values in sediments, depending on the $[H_2S]_{aq}$ level (Kerl et al. 2017). Alternatively, authigenic Mo can also be accumulated in reducing sediments via the Fe–Mn-oxyhydroxide particulate shuttle process: Fe- and Mn-oxyhydroxides adsorb the molybdate oxyanion in the oxic portion of the water column and transfer it to the sediment-water interface by particle sinking. Reductive dissolution of the particles then liberates Mo which may react with sulfide or organic matter or diffuse back into the water column (Algeo and Lyons 2006). Such cycling of Fe–Mn oxide particules in a weakly restricted redox-stratified ocean has been shown to generate Mo isotope signatures between the composition of seawater and oxic ferromanganese sediments (Kendall et al. 2017; Scholz et al. 2013; Noordmann et al. 2015).

Like Mo, U is also a conservative element with a residence time of ~ 400 kyr and a homogeneous distribution in the ocean (Ku et al. 1977). In modern oxic oceans, uranium occurs primarily in the highly soluble U^{6+} oxidation state, dominantly in the form of the uranyl carbonate complex $U^{VI}O_2(CO_3)_3^{4-}$. Biogenic carbonates and suboxic and anoxic sediments account for the main sinks of U in the modern ocean (Dunk et al. 2002). Modern seawater has a uniform $\delta^{238/235}$U of -0.39 ± 0.02‰ (Weyer et al. 2008; Tissot and Dauphas 2015; Andersen et al. 2017). Under oxic conditions, U can be removed from the water column by adsorption onto Fe–Mn-oxyhydroxide particles with relatively small isotopic fractionation from seawater of about −0.2‰ (Brennecka et al. 2011; Goto et al. 2014). In contrast, the reduction of U^{6+} to U^{4+} generates large isotopic fractionation of up to 1.2‰ (Fujii et al. 2006; Abe et al. 2008; Stylo et al. 2015; Wang et al. 2015), dominated by the nuclear field shift process. Uranium isotope fractionation has been traditionally suggested to mainly occur in reducing pore waters of sediments. While U precipitated by reduction of soluble U^{6+} to insoluble U^{4+} may result in a range of $\delta^{238/235}$U values from −0.4 to 0.6‰, many modern organic-rich sediments show $\delta^{238/235}$U between 0 and 0.2‰, equal to $\Delta^{238/235}U_{sediment\text{-}water}$ of ~ 0.6‰ (Andersen et al. 2014, 2017). This value is lower than the expected isotope fractionation induced by the nuclear field shift process and is likely muted by reactive transport during U diffusion in pore water in a closed system (Clark and Johnson 2008; Abe et al. 2008; Andersen et al. 2014). However, authigenic $\delta^{238/235}$U values higher than 0.2‰ are reported in some ancient black shales and modern analogs (e.g., Black Sea slope sediments or Eastern Mediterranean sapropels), suggesting that uranium reduction may occur both in the sediments and at the sediment-water interface (e.g., an organic flocculent layer) under open-system conditions. Such conditions could create uranium isotope fractionation of about 1.2‰ (Andersen et al. 2018, 2020; Brüske et al. 2020; Cheng et al. 2020; Kendall et al. 2020; Clarkson et al. 2023).

In this study, we analyzed Mo and U isotope compositions of the Early Cambrian polymetallic Ni–Mo-rich and V-rich black shale in South China to shed light on the Cambrian seawater redox conditions in marginal sea settings and their influence on the formation of the polymetallic Ni–Mo and V mineralization. These data are interpreted in combination with Mo and U isotope and elemental data on barren black shale from the same stratigraphic setting (Han et al. 2018; Cheng et al. 2020).

Geological background

The Early Cambrian black shales (Niutitang Formation and stratigraphic equivalents) in South China represent a condensed transgressive shelf sequence that is well exposed along the southeastern margin of the Yangtze

Platform. The Ediacaran-Cambrian paleogeographic reconstruction reveals shallow shelf facies of the karstic carbonate platform in the northwest toward transitional and deep basinal facies of black shale and chert in the southeast (Fig. 1(a), Zhu et al. 2003). Based on a comprehensive comparison of sections from the carbonate platform to the deep basin, Zhu et al. (2003) identified a protected offshore basin situation at the transitional zone with a peneplained hinterland that was separated to the southeastward open ocean by carbonate seamounts. The black shale sequence displays variable thickness from tens of meters to hundreds of meters. The Early Cambrian black shales of the Niutitang Formation unconformably overlie massive dolomite of the Neoproterozoic Dengying Formation and are overlain by clastic and carbonate sedimentary rocks. The unconformity has been taken as the Precambrian-Cambrian boundary at 542 Ma (Li et al. 2009).

The polymetallic Ni–Mo-rich and V-rich black shales occur along the NE-striking belt of the transitional zone. The former has a Re–Os isochron age of 521 ± 5 Ma (Xu et al. 2011), in agreement with a zircon SHRIMP U–Pb age of 532 ± 1 Ma for a volcanic ash bed below the Ni–Mo-rich layer (Jiang et al. 2009). A rough calculation indicates a sedimentation rate for the Ni–Mo-rich layer several hundred times lower than in modern euxinic sediments, such as in the Black Sea and the Cariaco basin (Lehmann et al. 2007, 2016). The polymetallic Ni–Mo-rich black shale occurs as a 3–20-cm-thick layer and has exceptionally high concentrations of Ni (up to 6.3 wt%) and Mo (up to 9.3 wt%). This layer is also rich in vanadium, uranium, selenium, and several other transition elements, as well as platinum group elements (PGEs) and Au (Coveney Jr. and Chen 1991; Steiner et al. 2001; Kříbek et al. 2007; Orberger et al. 2007; Xu et al. 2012, 2013). The black shale of the Niutitang Formation is overall vanadium enriched and locally hosts meter-thick shale units above the cut-off grade of about 0.5% V for economic mining in China. The ore-grade vanadium layers are reported as stratigraphically equivalent to the polymetallic Ni–Mo-rich layer (Xu and Mao 2021). A recent zircon U–Pb age of 521 ± 1 Ma (Wu et al. 2021) from a tuff layer interbedded with the vanadium ore at the Bagong mine, eastern Guizhou, is consistent with the age of the polymetallic Ni–Mo-rich layer (Xu et al. 2011). The polymetallic Ni–Mo-rich and V-rich black shales show a paleogeographically controlled zonation pattern. In the Zhangjiajie district, Hunan province, the polymetallic Ni–Mo-rich black shale (Sancha deposit) in the northeast grades into V-rich black shale (Xiongjiata deposit) in the southwest over a distance of about 25 km along strike (Fig. 1(b)).

Sampling details

We examined three categories of samples: polymetallic Ni–Mo-rich shale ($n = 11$), V-rich shale ($n = 9$), and their host black shales ($n = 10$, including one phosphorite sample). The polymetallic Ni–Mo-rich black shales are from the Maluhe (MLH) and Dazhuliushui (DZLS) mining districts in Guizhou province and the Sancha (SC) mine site in the Zhangjiajie district (Hunan province), which is ~ 400 km northeast of Dazhuliushui (Fig. 1(a)). Sampling at the Maluhe, Dazhuliushui, and Sancha mines includes the 3–5-cm-thick polymetallic Ni–Mo-rich black shales and the underlying and overlying host black shales. The V-rich samples were collected at the Xiongjiata mine (Zhangjiajie district), comprising the drill core ZK3001 and the Xiongjiata (XJT) road-cut samples (Fig. 1(b)). The Xiongjiata mine is ~ 20 km southwest of the Sancha polymetallic Ni–Mo-rich black shales. The total stratigraphic thickness of the V-rich black shales at the Xiongjiata mine in drill core ZK3001 and the road-cut section XJT are ~ 23 m and ~ 5 m, respectively. Samples from each section were collected to represent the full V-rich stratigraphic interval. All samples from Maluhe, Dazhuliushui, and Sancha were from underground mines. We carefully removed the superficial layer of samples from the Xiongjiata road-cut section to avoid the potential effects of weathering.

Analysis

Bulk sample geochemical analysis

Bulk samples of 0.5 to 1.0 kg weight were crushed, split, and subsequently powdered to ~ 200 mesh with an agate shatter box, prior to chemical analysis. The powdered bulk samples were analyzed for selected major and trace element compositions using a Finnigan MAT ELEMENT high-resolution ICP-MS at the Chinese National Research Center of Geoanalysis in Beijing, following Balaram et al. (1995) and Wu et al. (1996). Analytical reagent-grade HF and HNO_3 were used and purified before use by sub-boiling distillation. The PTFE pressure vessels were cleaned for 1 h using 20 vol% HNO_3 heated to 100 °C. Approximately 100 mg of powdered sample was digested with 1 mL HF and 0.5 mL HNO_3 in screw-top, PTFE-lined stainless pressure vessels at 190 °C for 12 h. The solution was then drained and evaporated to dryness with 0.5 mL HNO_3. This procedure was repeated twice. The final residue was re-dissolved by adding 8 mL of 40 vol% HNO_3. Subsequently, the pressure vessel was resealed and heated in an electric oven at 110 °C for 3 h. After cooling to room

temperature, the final solution was diluted to 100 mL by adding distilled de-ionized water. The reagent blanks were treated following the same procedures as the samples. Total analytical errors for trace elements in this study are within ± 6% (1 σ).

Mo isotope analysis

Molybdenum isotope measurements were done at the Institute of Geochemistry in Guiyang, China, with a Nu Plasma MC-ICP-MS following the methods of Wen et al. (2010, 2015). Molybdenum content was determined before isotope measurement. Powdered samples containing approximately > 100 ng Mo were oxidized at 400 °C for 6 h in an oven and then transferred to a Teflon beaker. The sample was digested using a mixture of HF and HNO_3 (1:2) at 100 °C for more than 16 h for complete sample dissolution. An updated anion/cation exchange resin double-column procedure designed by Zhang et al. (2009) was applied to yield an improved Mo recovery of 97.5 ± 0.3%. Column #1 was equipped with 5 mL 100–200 mesh Dowex AG 1-X8 resin and cleaned using 40 mL 1 M HCl. The column was washed with 20 mL 6 M HCl. Less than 3 mL sample solution was uploaded and rewashed with 30 mL 6 M HCl. Mo was finally collected by successively adding 45 mL 1 M HCl and 30 mL 5 M HNO_3. Column #2 was equipped with 3.5 mL 200–400 mesh Dowex AG 50W-X8 resin and cleaned with 30 mL 1.4 M HCl. Less than 2 mL sample solution was uploaded and collected with 11 mL 1.4 M HCl solution. This procedure provides for a negligible level of interference elements (e.g., Zr, Fe, and Mn) relative to Mo and uses a low volume of Mo elution solution. Mo isotope fractionation is negligible during sample dissolution and Mo purification (Zhang et al. 2009; Wen et al. 2010).

For Mo isotope measurement, samples were introduced into the MC-ICP-MS instrument in a free aspiration mode using a cyclonic chamber system equipped with a PFA pneumatic nebulizer. All samples and bracketing reference solutions were run in 2 blocks of 15 cycles of measurement on each amu. After each run, the nebulizer and spray chamber were rinsed with 0.6 M HNO_3 to obtain a stable signal of ^{96}Mo to the original background level. The standard-sample bracketing method was used to calculate delta values. A NIST SRM 3134 Mo solution (lot#891307) was used as an internal reference standard. The signal of a blank solution was subtracted for all measured masses, and instrumental drift was calibrated by averaging the measured ratios of the bracketing reference solution. A measured reference solution that presents linear or smooth drifting was considered for calculating sample delta values. Repeated measurements of pure Mo solutions yielded a reproducibility of better than ± 0.08‰, which was used as the analytical uncertainty for the rock samples. The $\delta^{98/95}Mo$ values are reported by + 0.25‰ for inter-lab comparison, as recommended by Nägler et al. (2014).

$$\delta^{98/95}\mathrm{Mo}\ (‰) = \left[\left({}^{98}\mathrm{Mo}/{}^{95}\mathrm{Mo}_{\mathrm{sample}}\right)/\left({}^{98}\mathrm{Mo}/{}^{95}\mathrm{Mo}_{\mathrm{NIST3134}}\right) - 1\right] \times 1000 + 0.25$$

U isotope analysis

For the chemical preparation of samples for U isotope analysis, approximately 200 mg powdered bulk sample was ashed in ceramic vessels at 550 °C overnight. The residue was digested with a concentrated HF/HNO_3/$HClO_4$ acid mixture (3:1:1) in Paar® high-pressure vessels at 180 °C. The samples were repeatedly treated with 6 M HNO_3 and 6 M HCl to dissolve any remaining fluorides. The samples were finally re-dissolved in 6 M HCl for U purification. The U double-spike IRMM 3636-A (^{236}U and ^{233}U mixture of 1:1, Richter et al. 2008) was added before separating U from the sample matrix by anion exchange chromatography, following the procedure described by Weyer et al. (2008).

All U isotope analyses (^{233}U, ^{235}U, ^{236}U, and ^{238}U) were conducted on a Thermo Scientific Neptune MC-ICP-MS at the Leibniz University of Hannover, using a Cetac Aridus system with a 50 µL PFA nebulizer for sample introduction, following the methods of Weyer et al. (2008), Montoya-Pino et al. (2010), and Noordmann et al. (2015). The ^{238}U isotope was measured on a 10^{10} Ω resistor, and the other three isotopes were measured on a 10^{11} Ω resistor due to their lower intensities. The U double-spike IRMM 3636-A was used to calibrate instrument mass bias during U isotope analysis. The spike/sample ratios were optimized to $n(^{236}U/^{233}U) \approx 3$, to minimize tailing effects from $n(^{238}U)$ on $n(^{236}U)$ and from $n(^{236}U)$ on $n(^{235}U)$, respectively. Uranium isotope analyses were obtained by standard bracketing relative to the U standard NBL CRM 112-A with a precision better than 0.05‰. The results of the isotope measurements are provided in the delta notation as follows:

$$\delta^{238/235}\mathrm{U}(‰) = \left[\left({}^{238}\mathrm{U}/{}^{235}\mathrm{U}_{\mathrm{sample}}\right)/\left({}^{238}\mathrm{U}/{}^{235}\mathrm{U}_{\mathrm{standard}}\right) - 1\right] \times 1000$$

Results

The chemical compositions of samples analyzed for Mo and U isotopes are listed in Table 1. The sulfidic polymetallic Ni–Mo-rich black shales (n = 11) have 3300–92,800 ppm Mo (mean: 57,200 ppm), 27,800–62,700 ppm Ni (mean:

Table 1 Elemental and Mo–U isotope data of the samples analyzed

Sample	Al_2O_3 (wt%)	U (ppm)	Mo (ppm)	Ni (ppm)	V (ppm)	P_2O_5 (wt%)	$U^{238/235}$	$\delta^{238/235}U_{measured}$ (‰)	2 σ	$U_{detrital}$ (%)	$\delta^{238/235}U_{authigenic}$ (‰)	$\delta^{98/95}Mo_{measured}$ (‰)	2 σ	$Mo_{detrital}$ (%)	$\delta^{98/95}Mo_{authigenic}$ (‰)
Polymetallic Ni–Mo-rich black shale															
MLH-2	3.26	118	61,600	37,700	480	0.64	137.8684	0.26	0.08	0.5	0.27				
MLH-5	1.71	112	70,900	36,300	423	0.51	137.8825	0.32	0.07	0.3	0.33				
MLH-10	1.70	109	66,900	42,600	329	0.70	137.8713	0.21	0.07	0.3	0.21	1.26	0.13	0	1.26
SC-2	1.20	408	56,400	61,500	1680	1.98	137.8786	0.27	0.05	0.1	0.27				
SC-5	1.37	396	3300	56,000	913	9.16	137.8377	0.02	0.02	0.1	0.02	0.50	0.02	0	0.50
SC-8	1.10	570	17,500	27,800	1210	16.3	137.8353	0.00	0.04	0	0.00	0.87	0.05	0	0.87
SC-11	1.32	595	65,900	29,900	3780	5.48	137.8940	0.42	0.05	0	0.42				
DZLS-2	1.29	125	73,100	62,700	658	0.85	137.8443	0.03	0.02	0.2	0.03				
DZLS-5	1.35	318	92,800	34,900	724	1.11	137.8639	0.18	0.11	0.1	0.18	1.20	0.14	0	1.20
DZLS-8	1.30	114	62,800	60,100	644	0.24	137.8989	0.43	0.05	0.2	0.43				
DZLS-11	0.88	255	57,600	46,100	486	1.80	137.8760	0.26	0.09	0.1	0.26	1.22	0.06	0	1.22
V-rich black shale															
ZK3001-1	8.12	42.6	60.0	213	2200	0.15	137.8656	0.22	0.03	3.5	0.24	0.73	0.13	1.3	0.74
ZK3001-2	6.98	64.3	134	317	7860	0.14	137.9181	0.60	0.04	2	0.62	0.12	0.06	0.5	0.12
ZK3001-4	10.7	48.0	111	242	2460	0.18	137.8745	0.26	0.01	4.1	0.28	0.65	0.09	1	0.65
ZK3001-5	7.67	66.3	123	289	2930	0.19	137.8845	0.33	0.04	2.1	0.34	0.21	0.07	0.6	0.21
ZK3001-6	7.52	46.0	210	320	2770	0.15	137.9192	0.59	0.04	3	0.61	0.29	0.08	0.4	0.29
XJT-2	9.88	177	370	442	5860	0.44	137.9271	0.61	0.03	1	0.62	0.76	0.10	0.3	0.76
XJT-5	5.30	60.7	18.0	84.5	1190	13.5	137.8293	−0.11	0.01	1.6	−0.10			2.9	
XJT-6	6.74	44.4	99.7	293	6770	0.14	137.9256	0.59	0.07	2.8	0.62	−0.24	0.08	0.7	−0.24
XJT-7	6.94	56.5	141	359	7100	0.11	137.9336	0.68	0.06	2.3	0.70	−0.27	0.06	0.5	−0.27
Host black shale															
MLH-4	14.2	54.9	142	301	310	0.21	137.8399	0.01	0.08	4.8	0.03				
MLH-6†	1.80	517	117	359	417	30.2	137.7677	−0.51	0.02	0.1	−0.51				
DZLS-7	12.1	30.6	65.2	332	409	0.15	137.8663	0.19	0.05	7.3	0.22				
DZLS-9	11.6	24.5	90.6	249	320	0.21	137.8742	0.25	0.06	8.8	0.30				
ZK3001-3	2.91	29.2	24.9	51.9	500	0.10	137.7960	−0.29	0.01	1.8	−0.29	2.22	0.09	1.2	2.24
ZK3001-7	8.34	74.4	180	269	847	0.23	137.8582	0.13	0.08	2.1	0.14	1.21	0.05	0.5	1.21
ZK3001-8	9.45	15.4	30.7	36.2	121	0.11	137.7840	−0.41	0.07	11.4	−0.42	2.54	0.04	3.1	2.61
XJT-1	11.7	16.6	10.0	102	667	0.20	137.8245	−0.11	0.07	13.1	−0.08	0.93	0.07	11.7	1.01
XJT-3	13.1	8.30	2.70	95.6	165	0.11	137.8948	0.37	0.06	29.1	0.65	0.49	0.16	48	0.67
XJT-4	13.6	33.6	13.5	94.1	599	0.18	137.8732	0.21	0.06	7.5	0.25			10	

†Phosphorite

45,100 ppm), and 109–595 ppm U (mean: 284 ppm), much higher than that of the V-rich black shales ($n = 9$), which have 18.0–370 ppm Mo (mean: 141 ppm), 84.5–442 ppm Ni (mean: 284 ppm), and 42.6–177 ppm U (mean: 67.3 ppm). In contrast, the V-rich black shales have higher V concentrations of 1190–7860 ppm (mean: 4350 ppm) than that of the Ni–Mo-rich samples of 329–3780 (mean: 1030 ppm). Compared to the Ni–Mo-rich and V-rich black shales, the barren black shales have relatively lower Mo, Ni, U, and V, with 2.70–180 ppm Mo (mean: 67.7 ppm), 36.2–359 ppm Ni (mean: 189 ppm), 8.30–517 ppm U (mean: 80.5 ppm), and 121–847 ppm V (mean: 436 ppm).

The Mo and U isotope data are presented in Table 1. The isotope data are plotted in Fig. 2 together with the dataset from Xu et al. (2012) and Cheng et al. (2020). The sample set shows an overall inverse covariation pattern of Mo versus U isotope data ($R^2 = 0.55$). The sulfidic polymetallic Ni–Mo-rich samples have authigenic $\delta^{98/95}$Mo values ranging from 0.50 to 1.38‰ (mean: 1.1 ± 0.2‰, 1 σ) and authigenic $\delta^{238/235}$U values from 0 to 0.43‰ (mean: 0.2 ± 0.1‰, 1 σ). The V-rich shale samples have variable but low $\delta^{98/95}$Mo values from −0.27 to 0.76‰ (mean: 0.3 ± 0.4‰, 1 σ) and elevated authigenic $\delta^{238/235}$U values from −0.10 to 0.70‰ (mean: 0.4 ± 0.2‰, 1 σ). The barren black shale samples display a large spread of Mo and U isotope data with $\delta^{98/95}$Mo ranging from 0.67 to 2.61‰ (mean: 1.5 ± 0.6‰, 1 σ) and $\delta^{238/235}$U ranging from −0.51 to 0.65‰ (mean: 0 ± 0.3‰, 1 σ).

The inverse correlation of Mo and U isotope compositions (Fig. 2) is more significant ($R^2 = 0.68$), if excluding three samples with elevated P content from 9–30 wt% P_2O_5 (corresponding to 23–75 wt% apatite, Fig. 2). These samples reflect an external bioclastic component from a suboxic distal slope environment (Kříbek et al. 2007). The sample with the lowest $\delta^{238/235}$U value of −0.51‰ is phosphorite.

Discussion

Detrital vs. authigenic components

The Mo and U concentrations and their isotope compositions in sediments deposited in oceanic basins are a mixture of detrital input and authigenic metal enrichment (Asael et al. 2013; Noordmann et al. 2015). Before using Mo and U concentrations and their isotope composition as tracers of paleo-ocean redox conditions, it is essential to estimate the contributions of detrital and authigenic fractions, as only authigenic fractions are meaningful for paleoenvironmental interpretations. In the detrital lithogenic component, U and Mo are physically transported and deposited as a solid phase. The U in authigenic phases may be associated with biogenic carbonate or organic biomass or derived from reductive authigenic precipitation from pore waters (Dunk et al. 2002). Mo in authigenic phases is associated with molybdate or thiomolybdate. The detrital component in sediments is often estimated by normalization to Al content and assumed lithogenic U/Al and Mo/Al ratios. The authigenic components are calculated by the following equations:

$$\mathrm{Mo}_{\mathrm{authigenic}} = \mathrm{Mo}_{\mathrm{measured}} - \left(\mathrm{Mo}_{\mathrm{ucc}}/\mathrm{Al}_{\mathrm{ucc}} \times \mathrm{Al}_{\mathrm{measured}}\right)$$

$$\mathrm{U}_{\mathrm{authigenic}} = \mathrm{U}_{\mathrm{measured}} - \left(\mathrm{U}_{\mathrm{ucc}}/\mathrm{Al}_{\mathrm{ucc}} \times \mathrm{Al}_{\mathrm{measured}}\right)$$

To estimate the detrital component of U and Mo of our samples, we use [Al] = 8 wt%, [U] = 2.8 ppm, and [Mo] = 1.5 ppm of average upper continental crust (UCC) as suggested by Taylor and McLennan (1995). Based on the isotopic mass balance, authigenic Mo and U isotope compositions can be calculated by the following equations:

$$\delta^{98/95}\mathrm{Mo}_{\mathrm{authigenic}} = \left(\delta^{98/95}\mathrm{Mo}_{\mathrm{measured}} \times \mathrm{Mo}_{\mathrm{measured}} - \delta^{98}\mathrm{Mo}_{\mathrm{detrital}} \times \mathrm{Mo}_{\mathrm{detrital}}\right)/\mathrm{Mo}_{\mathrm{authigenic}}$$

$$\delta^{238/238}\mathrm{U}_{\mathrm{authigenic}} = \left(\delta^{238/235}\mathrm{U}_{\mathrm{measured}} \times \mathrm{U}_{\mathrm{measured}} - \delta^{238}\mathrm{U}_{\mathrm{detrital}} \times \mathrm{U}_{\mathrm{detrital}}\right)/\mathrm{U}_{\mathrm{authigenic}}$$

In the above equations, $\mathrm{Mo}_{\mathrm{detrital}} = \mathrm{Mo}_{\mathrm{ucc}}/\mathrm{Al}_{\mathrm{ucc}} \times \mathrm{Al}_{\mathrm{measured}}$ and $\mathrm{U}_{\mathrm{detrital}} = \mathrm{U}_{\mathrm{ucc}}/\mathrm{Al}_{\mathrm{ucc}} \times \mathrm{Al}_{\mathrm{measured}}$, respectively. We use $\delta^{98/95}\mathrm{Mo}_{\mathrm{detrital}} = 0.3‰$ (Voegelin et al. 2014) and $\delta^{238/235}\mathrm{U}_{\mathrm{detrital}} = -0.30‰$, respectively (Tissot and Dauphas 2015; Noordmann et al. 2016), for the isotope composition of the detrital component.

The detrital contributions are very low for all polymetallic Ni–Mo-rich samples (< 0.5% of total Mo and U, respectively, Table 1), in line with a very low clastic sedimentation rate (Lehmann et al. 2016). Although the detrital components of the V-rich black shales are slightly higher than that of the polymetallic Ni–Mo-rich samples, they are still low, with less than 3 wt% detrital Mo and 5 wt% detrital U. The authigenic metal components are also dominant in the barren black shale, but a few samples have significant detrital Mo and V. For example, sample XJT-3 from the Xiongjiata road-cut contains as much as 48% detrital Mo and 29% detrital U. In combination with detrital Mo and detrital U calculation, we infer that the host black shale samples from the Xiongjiata drill core (XJT samples) have relatively larger detrital components than the host black shales from other sites. Because of the overall low detrital contributions,

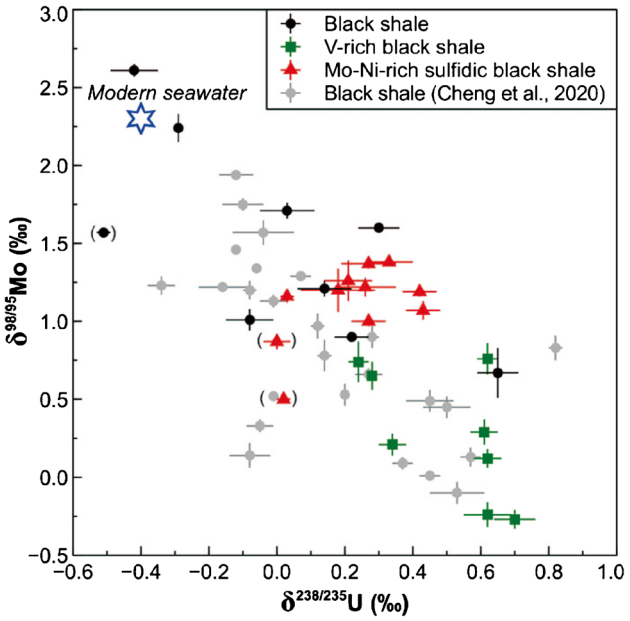

Fig. 2 Plot of $\delta^{238/235}U$ versus $\delta^{98/95}Mo$ for the polymetallic Ni–Mo-rich shale, V-rich shale, and the host barren black shale from the southeastern margin of the Yangtze Platform, South China. Modern seawater isotope composition of Mo and U according to Kendall et al. (2017) and Andersen et al. (2017), respectively. Three P-rich samples (9–30 wt% P_2O_5) deviate from the trend and are indicated by brackets

the calculated authigenic Mo and U isotope values are very close to the measured values but with the exception of sample XJT-3 with significant detrital U and Mo.

Heterogeneity of the marginal sea and its influence on the Mo (Ni)–V mineralization

The U isotopic composition of Early Cambrian seawater was likely similar to present-day, considering it was dominantly oxidized (Chen et al. 2015). The highly metalliferous Mo–Ni- and V-rich shale units are within a > 100-m-thick black shale sequence with $\delta^{98/95}Mo$ up to 2.6‰ and $\delta^{238/235}U$ as low as −0.5‰ (Fig. 2). These values are close to those of modern seawater. This suggests that (1) Early Cambrian seawater may have had a similar Mo and U isotope composition to modern seawater which would require significant Mo and U sinks in oxic or suboxic environments; (2) both Mo and U were almost quantitatively scavenged from seawater, in an environment similar to the Black Sea, with euxinic conditions characterized by elevated H_2S in the water column. Such a redox-stratified paleo-ocean is also suggested by Se, Hg, Cr, and Cd isotopes from black shales of the Niutitang Formation (Wen and Carignan 2011; Yin et al. 2017; Frei et al. 2021). However, most of our black shale samples display significant Mo and U isotope fractionation relative to modern seawater and hypothetical Early Cambrian seawater.

The V-rich shale unit displays relatively light Mo isotope and heavy U isotope compositions (Fig. 2), resulting in correlated Mo and U isotope fractionation relative to seawater during Mo and U reduction and deposition. The light Mo isotope composition is consistent with Mo scavenging under anoxic depositional conditions of the V-rich shale, resulting in significant Mo isotope fractionation. The heavy U isotope composition implies that U reduction likely occurred in an open system such as the bottom water column or at the water-sediment interface. This is different from recent organic-rich shales where a relatively constant U isotope fractionation of up to 0.6‰ is typically observed and interpreted to be the result of diffusion-limited U isotope fractionation during U reduction in the sediment pore water (Andersen et al. 2014, 2018; Brüske et al. 2020). In contrast, larger U isotope fractionation up to the theoretical limit of 1.2‰ may occur during U reduction in the water column or near a bottom floating flocculent layer of organic material in an open system (Andersen et al. 2020; Brüske et al. 2020; Cheng et al. 2020; Clarkson et al. 2023).

In contrast to the V-rich black shales, the Mo–Ni-rich sulfidic black shale has an intermediate Mo and U isotope composition. Given the extreme enrichment of Mo and Ni, this shale unit represents an unusually efficient case of metal scavenging which has been much debated in the literature (Lehmann et al. 2022). Intriguingly, this unit is significantly fractionated in Mo and Ni isotope composition compared to modern seawater and some barren black shale samples, with $\Delta^{98/95}Mo_{sample\text{-}seawater}$ of about −1‰ (Lehmann et al. 2007; Xu et al. 2012) and $\Delta^{60/58}Ni_{sample\text{-}seawater}$ of about −1 to −2‰ (Pašava et al. 2019) but also with respect to euxinic sediments in general. The distinct Mo and Ni signature may be the result of a ferromanganese oxyhydroxide particulate shuttle process, which can imprint a shift of $\delta^{98/95}Mo$ and $\delta^{60/58}Ni$ toward lower values (Goldberg et al. 2009; Kendall et al. 2017; Little et al. 2020), because of the high Mo concentration and light Mo isotope composition of manganese oxyhydroxides (Barling and Anbar 2004). In addition, it has been shown experimentally that iron oxyhydroxides, such as goethite and ferrihydrite, also fractionate Mo isotopes by about −1.0 to −1.5‰ (Goldberg et al. 2009). Manganese oxides also fractionate Ni isotopes by about −3‰ (Sorensen et al. 2020). During the particulate shuttle process, particle-reactive elements, such as Mo and Ni, are adsorbed by Fe–Mn-oxyhydroxide particles in the oxic zone. These particles, enriched in isotopically light Mo and Ni, would then settle through the water column and release these metals under reducing conditions in the euxinic bottom water where they are fixed as sulfides. Isotopic mass balance modeling demonstrates that the Fe–Mn-oxyhydroxide shuttle on euxinic continental margins can bury isotopically light Mo and significantly modify the Mo isotope composition of the water column (Qin et al. 2022). The low Mn bulk content of

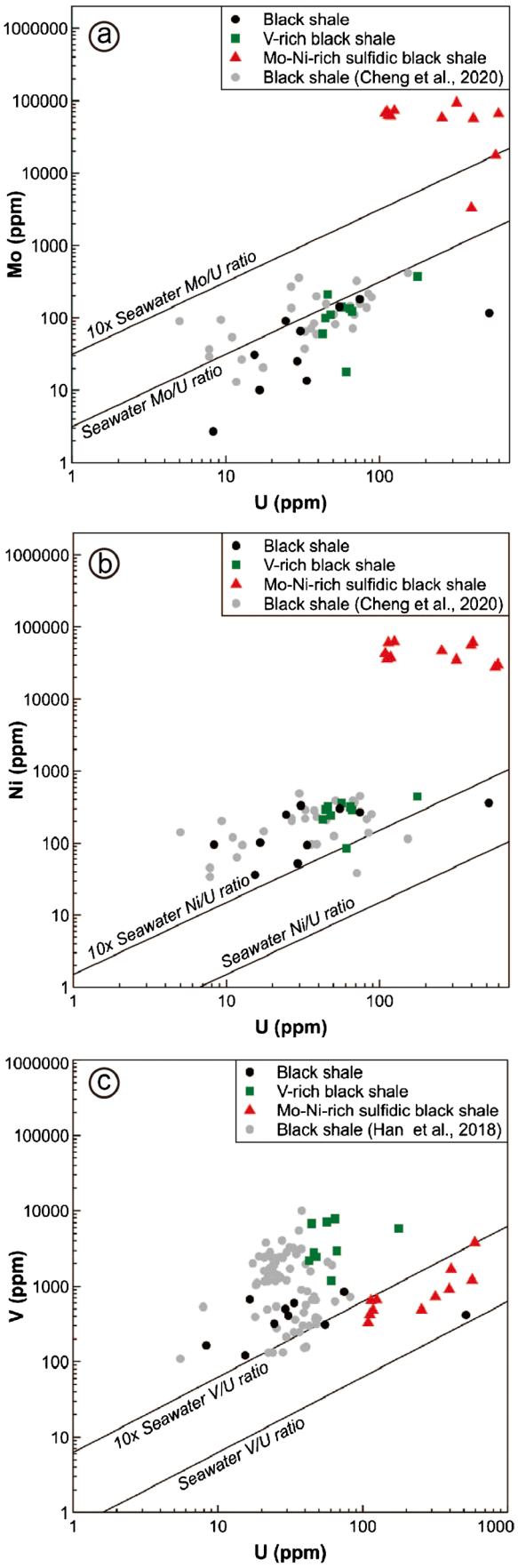

Fig. 3 **a–c** Mo–Ni–V–U relationships in the Early Cambrian black shale sequence on the Yangtze Platform. Note the deviation of the Mo–U and Ni–U trends for the samples of Mo–Ni-rich sulfidic black shale, attributed to enhanced accumulation of authigenic Mo and Ni over U due to particulate shuttle process. The enrichment of V in the vanadium-rich shale is in line with the barren black shale and suggests that the V-rich shale is part of the normal black shale population, but with less clastic dilution

the euxinic sediments can be explained by reductive dissolution of the Mn component which is cycled out of the system, while Fe becomes fixed as pyrite.

The negative correlation between $\delta^{98/95}$Mo and $\delta^{238/238}$U indicates changes in the local depositional environment, different from the expected positive correlation for global ocean redox variations (Kendall et al. 2020). Such an inverse correlation of Mo and U isotope compositions is not only observed in the Early Cambrian black shales in South China but also in organic-rich shales that formed in local (semi-)restricted basins throughout geological history (Asael et al. 2013; Kendall et al. 2015, 2020; Andersen et al. 2020; Brüske et al. 2020; Li et al. 2022). The inverse correlation could be attributed to changes in dissolved sulfide concentrations and sulfate reduction rates related to deep water renewal rates and metal removal to sediment (Bura-Nakić et al. 2018). In restricted basins, the renewal rate of deep water would be lower than that of shallow water. Shales deposited under reducing deep water conditions with porewater of high sulfide concentrations have isotopically unfractionated Mo due to quantitative transformation from molybdate to thiomolybdate. However, these shales are depleted in ^{238}U because of U reduction and removal to sediments (Li et al. 2022). In contrast, shallow sedimentary basins with a better connection to the open ocean have a faster bottom water renewal rate. As a result, the transformation from molybdate to thiomolybdate in the water column would be less quantitative, and U reduction and removal to sediments would be less efficient. Shales formed under such conditions, therefore, have lower $\delta^{98/95}$Mo and higher $\delta^{238/235}$U values. The commonly observed inverse correlations of Mo and U isotopes in black shales demonstrate that local (semi-) restricted basins were not rare in geological history (Asael et al. 2013; Andersen et al. 2020; Brüske et al. 2020; Kendall et al. 2015, 2020; Li et al. 2022).

The Mo–Ni–V–U inter-element relationships in Fig. 3a–c display the extreme enrichment of Mo and Ni in the sulfidic black shale. This is different from the non-sulfidic V-rich shale which displays enrichment patterns in Ni, Mo, and V with respect to U which are less extreme and which are continuous with barren black shale. The deviation in Mo and Ni in the Ni–Mo sulfide unit (Mo and Ni in the percent range) by up to two orders of magnitude from normal black shales requires a specific enrichment process, which could be the Fe–Mn-oxyhydroxide particulate shuttle described above.

Fast accumulation of authigenic Mo over authigenic U by about one order of magnitude, associated with Fe–Mn redox cycling, was observed in the Cariaco basin, Venezuela, and the Gotland Deep of the Baltic Sea between Sweden and the Baltic countries (Algeo and Tribovillard 2009; Scholz et al. 2013).

While the Mo/U ratio of the normal black shale and the V-rich shale crudely reflects the Mo/U ratio of seawater, their Ni/U ratio is 10–100 times more elevated than in seawater but is close to the Ni/U ratio in marine microbiota (Miyake et al. 1970; Piper 1994), which suggests that part of the Ni component could be of biogenic origin, released during mineralization of organic material. The anoxic V-rich shale did not form in the sulfidic environment required for the fixation of Mo and Ni, and these metals are then cycled back to seawater. In addition to elevated Ni/U ratios, the V-rich shale also has V/U ratios above seawater, which are close to those of marine microbiota (Miyake et al. 1970; Piper 1994). The fixation of V depends on the Al content, because V is fixed in a variety of clay minerals under anoxic conditions. The V enrichment process seems to be the same as for normal black shale, because both rock units are on the same V-U correlation trend (Fig. 3c) but with more pronounced V and U enrichment in the ore-grade units.

A refined metallogenic model

Although the Early Cambrian seawater on the continental margins of the Yangtze Platform was dominantly oxidized (Chen et al. 2015), the rifted margin and its karstic geography created semi-restricted basins with variably reducing conditions and low clastic sedimentation. Upwelling of deep ocean water along the continental margin allowed high bioproductivity in the photic zone and a rain of biological debris, which led to sulfidic bottom water conditions in restricted basins (Fig. 4). The water column was redox-stratified, and possibly also salinity-stratified, given the paleogeographic setting (near-equatorial restricted basins), which favors vertical particulate cycling (Algeo and Lyons 2006; Goldberg et al. 2009; Cheng et al. 2020). The particle-reactive Mo and Ni were captured by Fe–Mn-oxyhydroxide particules in the oxic zone which settled down into the euxinic bottom waters, where Mo and Ni were released, and Fe, Mo, and Ni were fixed as sulfide. The sulfide concentration was likely insufficient to form alabandite (MnS), which requires extremely low fO_2, and thus, Mn was cycled out of the system. Locally strong bottom currents are indicated by textural features such as synsedimentary clasts of organic material and sulfides in a pyrobitumen-sulfide-clay matrix (Steiner et al. 2001) and reworked subaquatic phosphatic hardground (Kříbek et al. 2007). The "ferromanganese oxyhydroxide shuttle" (Goldberg et al. 2009) was likely a major vector to imprint the relatively light Mo and Ni isotope composition on the sulfide-rich bottom sediments. These sediments may also have a Mo component from quantitative Mo scavenging directly from seawater by sulfide particles and became isotopically homogenized at and below the sediment interface.

Such conditions of a starved redox-stratified basin with elevated biological productivity in the photic zone also favor the enrichment of vanadium in the clay fraction of the sediment. However, unlike Mo that is only fixed as tetra-thiomolybdate under strongly euxinic conditions, vanadium enrichment can occur under anoxic/moderately euxinic or even suboxic conditions by adsorption of the $[VO(OH)]_3^-$ complex on clay minerals (Emerson and Huested 1991). In such spatially broader suboxic to anoxic environments, Mo and U remain in the water column due to the lack of a sufficiently low oxidation state with high H_2S activity. The V enrichment

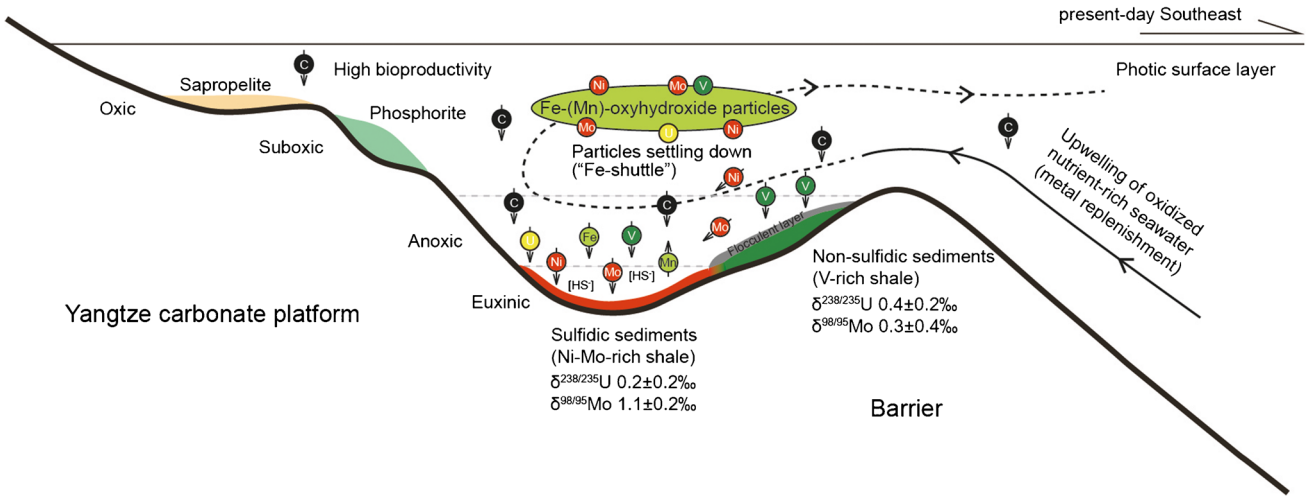

Fig. 4 A schematic model for the Early Cambrian paleoceanographic situation at the margin of the Yangtze Platform, South China, and redox control of the polymetallic Ni–Mo and V mineralization

process is continuous with the distribution of black shale and mainly reflects the sediment accumulation rate.

Conclusions

The inversely correlated Mo and U isotope data from Early Cambrian black shales on the Yangtze Platform identify a diverse spectrum of local depositional environments in biologically highly productive and physically dynamic redox-stratified marginal basins. Polymetallic sulfidic units suggest quantitative Mo and U removal from euxinic bottom water fed by the adsorbed metal load of vertically cycling ferromanganese oxide particules. Less quantitative Mo and U removal from anoxic or weakly sulfidic bottom water and sediment pore water resulted in large sediment-seawater isotope fractionation with lighter Mo and heavier U isotopes, accompanied by efficient V enrichment. Both end-member variants may occur in temporally and spatially variable proportions in fluctuating paleohydrographic settings within the same stratigraphic sequence, such as on the Neoproterozoic/Early Cambrian Yangtze Platform, or in some Early Paleozoic marginal basins in North America (Gadd et al. 2020; Crawford et al. 2021). Coupled Mo and U isotope data from Early Cambrian metalliferous black shales on the Yangtze Platform show temporally and spatially variable hydrodynamic/environmental conditions in a marginal basin with starved clastic deposition but with elevated bioproductivity. The black shale host sequence shows an inverse correlation trend of Mo and U isotope composition similar to modern environments, and we infer that the global Early Cambrian seawater was at least episodically similar to modern seawater, with dominantly oxic Mo sinks in the oceans.

Acknowledgements This work was supported by the National Natural Science Foundation of China (grant 41972072, 42172080). We are grateful to three anonymous referees and Associate Editor Frank Melcher for their thorough reviews.

Declarations

Conflict of interest The authors declare no competing interests.

References

Abe M, Suzuki T, Fujii Y, Hada M, Hirao K (2008) An ab initio molecular orbital study of the nuclear volume effect in uranium isotope fractionations. J Chem Phys 129:164309

Algeo TJ, Lyons TW (2006) Mo−total organic carbon covariation in anoxic mrine environments: implications for analysis of paleoredox and paleohydrographic conditions. Paloceanography 21:PA1016

Algeo TJ, Tribovillard N (2009) Environmental analysis of paleoceanographic systems based on molybdenum–uranium covariation. Chem Geol 268:211–225

Andersen MB, Matthews A, Bar-Matthews M, Vance D (2020) Rapid onset of ocean anoxia shown by high U and low Mo isotope compositions of sapropel S1. Geochem Perspect Lett 15:10–14

Andersen MB, Matthews A, Vance D, Bar-Matthews M, Archer C, de Souza GF (2018) A 10-fold decline in the deep Eastern Mediterranean thermohaline overturning circulation during the last interglacial period. Earth Planet Sci Lett 503:58–67

Andersen MB, Romaniello S, Vance D, Little SH, Herdman R, Lyons TW (2014) A modern framework for the interpretation of $^{238}U/^{235}U$ in studies of ancient ocean redox. Earth Planet Sci Lett 400:184–194

Andersen MB, Stirling CH, Weyer S (2017) Uranium isotope fractionation. Rev Mineral Geochem 82:799–850

Asael D, Tissot FLH, Reinhard CT, Rouxel O, Dauphas N, Lyons TW, Ponzevera E, Liorzou C, Chéron S (2013) Coupled molybdenum, iron and uranium stable isotopes as oceanic paleoredox proxies during the Paleoproterozoic Shunga Event. Chem Geol 362:193–210

Balaram V, Anjaiah KV, Reddy MRP (1995) Comparative study on the trace and rare earth element analysis of an Indian polymetallic nodule reference sample by inductively coupled plasma atomic emission spectrometry and inductively coupled plasma mass spectrometry. Analyst 120:1401–1406

Barling J, Anbar AD (2004) Molybdenum isotope fractionation during adsorption by manganese oxides. Earth Planet Sci Lett 217:315–329

Barling J, Arnold GL, Anbar AD (2001) Natural mass-dependent variations in the isotopic composition of molybdenum. Earth Planet Sci Lett 193:447–457

Brennecka GA, Wasylenki LE, Bargar JR, Weyer S, Anbar AD (2011) Uranium isotope fractionation during adsorption to Mn-oxyhydroxides. Environ Sci Technol 45:1370–1375

Brüske A, Weyer S, Zhao MY, Planavsky NJ, Wegwerth A, Neubert N, Dellwig O, Lau KV, Lyons TW (2020) Correlated molybdenum and uranium isotope signatures in modern anoxic sediments: Implications for their use as paleo-redox proxy. Geochim Cosmochim Acta 270:449–474

Bura-Nakić E, Andersen MB, Archer C, de Souza GF, Marguš M, Vance D (2018) Coupled Mo-U abundances and isotopes in a small marine euxinic basin: constraints on processes in euxinic basins. Geochim Cosmochim Acta 222:212–229

Chen X, Ling HF, Vance D, Shields-Zhou GA, Zhu MY, Poulton SW, Och LM, Jiang SY, Li D, Cremonese L, Archer C (2015) Rise to modern levels of ocean oxygenation coincided with the Cambrian radiation of animals. Nat Commun 6:7142

Cheng M, Li C, Jin CS, Wang HY, Algeo TJ, Lyons TW, Zhang FF, Anbar A (2020) Evidence for high organic carbon export to the early Cambrian seafloor. Geochim Cosmochim Acta 287:125–140

Clark SK, Johnson TM (2008) Effective isotopic fractionation factors for solute removal by reactive sediments: a laboratory microcosm and slurry study. Environ Sci Technol 42:7850–7855

Clarkson MO, Sweere TC, Chiu CF, Hennekam R, Bowyer F, Wood RA (2023) Environmental controls on very high $\delta^{238}U$ values in reducing sediments: implications for Neoproterozoic seawater records. Earth Sci Rev 237:104306

Coveney RM Jr, Chen N (1991) Ni-Mo-PGE-Au-rich ores in Chinese black shales and speculations on possible analogues in the United States. Mineral Deposita 26:83–88

Coveney RM Jr, Grauch RI, Murowchick JB (1994) Metals, phosphate and stone coal in the Proterozoic and Cambrian of China: the geologic setting of precious metal-bearing Ni-Mo ore beds. Soc Econ Geol Newsl 18:6–11

Crawford I, Layton-Matthews D, Peter JM, Gadd MG, Voinot A, Leybourne MI, Pufahl P (2021) Application of molybdenum and thallium isotopes as indicators of paleoredox conditions and genesis

of hyper-enriched black shale deposits, Peel river, Yukon, Canada. Can Mineral 59:1085–1110
Dunk RM, Mills RA, Jenkins WJ (2002) A reevaluation of the oceanic uranium budget for the Holocene. Chem Geol 190:45–67
Emerson SR, Huested SS (1991) Ocean anoxia and the concentrations of molybdenum and vanadium in seawater. Mar Chem 34:177–196
Frei R, Xu L, Frederiksen JA, Lehmann B (2021) Signals of combined chromium-cadmium isotopes in basin waters of the Early Cambrian – results from the Maoshi and Zhijin sections, Yangtze Platform. South China Chem Geol 563:120061
Fujii Y, Higuchi N, Haruno Y, Nomura M, Suzuki T (2006) Temperature dependence of isotope effects in uranium chemical exchange reactions. J Nucl Sci Technol 43:400–406
Gadd MG, Peter JM, Hnatyshin D, Creaser R, Gouwy S, Fraser T (2020) A Middle Devonian basin-scale precious metal enrichment event across northern Yukon (Canada). Geology 48:242–246
Goldberg T, Archer C, Cance D, Poulton SW (2009) Mo isotope fractionation during adsorption to Fe (oxyhydr)oxides. Geochim Cosmochim Acta 73:6502–6516
Goto KT, Anbar AD, Gordon GW, Romaniello SJ, Shimoda G, Takaya Y, Tokumaru A, Nozaki T, Suzuki K, Machida S, Hanyu T, Usui A (2014) Uranium isotope systematics of ferromanganese crusts in the Pacific Ocean: implications for the marine $^{238}U/^{235}U$ isotope system. Geochim Cosmochim Acta 146:43–58
Han T, Fan HF, Wen HJ (2018) Dwindling vanadium in seawater during the early Cambrian, South China. Chem Geol 492:20–29
Jiang SY, Pi DH, Heubeck C, Frimmel H, Liu YP, Deng HL, Ling HF, Yang JH (2009) Early Cambrian ocean anoxia in South China. Nature 459:E5–E6
Kendall B, Dahl TW, Anbar AD (2017) The stable isotope geochemistry of molybdenum. Rev Mineral Geochem 82:683–732
Kendall B, Komiya T, Lyons TW, Bates SM, Gordon GW, Romaniello SJ, Jiang G, Creaser RA, Xiao S, McFadden K, Sawaki Y, Tahata M, Shu D, Han J, Li Y, Chu X, Anbar AD (2015) Uranium and molybdenum isotope evidence for an episode of widespread ocean oxygenation during the Late Ediacaran Period. Geochim Cosmochim Acta 156:175–193
Kendall B, Wang JY, Zheng W, Romaniello SJ, Over DJ, Bennett Y, Xing LY, Kunert A, Boyes C, Liu J (2020) Inverse correlation between the molybdenum and uranium isotope compositions of Upper Devonian black shales caused by changes in local depositional conditions rather than global ocean redox variations. Geochim Cosmochim Acta 287:141–164
Kerl CF, Lohmayer R, Bura-Nakić E, Vance D, Planer-Friedrich B (2017) Experimental confirmation of isotope fractionation in thiomolybdates using ion chromatographic separation and detection by multi-collector ICP-MS. Anal Chem 89:3123–3129
Knoll AH, Carroll SB (1999) Early animal evolution: emerging views from comparative biology and geology. Science 284:2129–2137
Kříbek B, Sýkorová I, Pašava J, Machovič V (2007) Organic geochemistry and petrology of barren and Mo-Ni-PGE mineralized marine black shales of the Lower Cambrian Niutitang Formation (South China). Int J Coal Geol 72:240–256
Ku TL, Knauss KG, Mathieu GG (1977) Uranium in open ocean – concentration and isotopic composition. Deep-Sea Res 24:1005–1017
Lehmann B, Frei R, Xu LG, Mao JW (2016) Early Cambrian black shale-hosted Ni-Mo and V mineralization on the rifted margin of the Yangtze Platform, China: reconnaissance chromium isotope data and a refined metallogenic model. Econ Geol 111:89–103
Lehmann B, Nägler TF, Holland HD, Wille M, Mao JW, Pan JY, Ma DS, Dulski P (2007) Highly metalliferous carbonaceous shale and Early Cambrian seawater. Geology 35:403–406
Lehmann B, Pašava J, Šebek O, Andronikov A, Frei R, Xu L, Mao J (2022) Early Cambrian highly metalliferous black shale in South China: Cu and Zn isotopes and a short review of other non-traditional stable isotopes. Mineral Deposita 57:1167–1187
Li D, Ling HF, Jiang SY, Pan JY, Cheng YQ, Cai YF, Feng HZ (2009) New carbon isotope stratigraphy of the Ediacaran-Cambrian boundary interval from SW China: implications for global correlation. Geol Mag 146:465–484
Li J, Azmy K, Kendall B (2022) The Mo- and U-isotope signatures in alternating shales and carbonate beds of rhythmites: a comparison and implications for redox conditions across the Cambrian-Ordovician boundary. Chem Geol 602:120882
Little SH, Archer C, McManus J, Najorka J, Wegorzewaki AV, Vance D (2020) Towards balancing the oceanic Ni budget. Earth Planet Sci Lett 547:116461
Mao JW, Lehmann B, Du AD, Zhang GD, Ma DS, Wang YT, Zeng MG, Kerrich R (2002) Re-Os dating of polymetallic Ni-Mo-PGE-Au mineralization in Lower Cambrian black shales of South China and its geologic significance. Econ Geol 97:1051–1061
Miyake Y, Sugimura Y, Mayeda M (1970) The uranium content and the activity ratio $^{234}U/^{238}U$ in marine organisms and sea water in the western North Pacific. J Oceanogr Soc Japan 26:123–129
Montoya-Pino C, Weyer S, Anbar AD, Pross J, Oschmann W, van de Schootbrugge B, Arz HW (2010) Global enhancement of ocean anoxic during oceanic anoxic event 2: a quantitative approach using U isotopes. Geology 38:315–318
Nägler TF, Anbar AD, Archer C, Goldberg T, Gordon GW, Greber ND, Siebert C, Sohrin Y, Vance D (2014) Proposal for an international molybdenum isotope measurement standard and data representation. Geostand Geoanal Res 38:149–151
Neubert N, Nägler TF, Böttcher ME (2008) Sulfidity controls molybdenum isotope fractionation into euxinic sediments: evidence from the modern Black Sea. Geology 36:775–778
Noordmann J, Weyer S, Georg RB, Jöns S, Sharma M (2016) $^{238}U/^{235}U$ isotope ratios of crustal material, rivers and products of hydrothermal alteration: new insights on the oceanic U isotope mass balance. Isot Environ Health Stud. https://doi.org/10.1080/10256016.2015.1047449
Noordmann J, Weyer S, Montoya-Pino C, Dwelling O, Neubert N, Eckardt S, Paetzel M, Böttcher M (2015) Uranium and molybdenum isotope systematics in modern anoxic basins: case studies from the Central Baltic Sea and the Kyllaren fjord (Norway). Chem Geol 396:182–195
Orberger B, Vymazalova A, Wagner C, Fialin M, Gallien JP, Wirth R, Pašava J, Montagnac G (2007) Biogenic origin of intergrown Mo-sulfide-and carbonaceous matter in Lower Cambrian black shales (Zunyi Formation, southern China). Chem Geol 238:213–231
Pašava J, Chrastný V, Loukola-Ruskeeniemi K, Šebek O (2019) Nickel isotopic variation in black shales from Bohemia, China, Canada, and Finland: a reconnaissance study. Mineral Deposita 54:719–742
Piper DZ (1994) Seawater as the source of minor elements in black shales, phosphorites, and other sedimentary rocks. Chem Geol 114:95–114
Qin Z, Xu D, Kendall B, Zhang X, Qu Q, Wang X, Li J, Liu J (2022) Molybdenum isotope-based redox deviation driven by continental margin euxinia during the early Cambrian. Geochim Cosmochim Acta 325:152–169
Richter S, Alonso-Munoz A, Eykens R, Jacobsson U, Kuehn H, Verbruggen A, Aregbe Y, Wellum R, Keegan E (2008) The isotopic composition of natural uranium samples – measurements using the new $n(^{233}U)/n(^{236}U)$ double spike IRMM-3636. Int J Mass Spectrom 269:145–148
Scholz F, McManus J, Sommer S (2013) The manganese and iron shuttle in a modern euxinic basin and implications for molybdenum cycling at euxinic ocean margins. Chem Geol 355:56–68

Sorensen JV, Gueguen B, Stewart BD, Peña J, Rouxel O, Toner BM (2020) Large nickel isotope fractionation caused by surface complexation reactions with hexagonal birnessite. Chem Geol 537:119481

Sperling EA, Frieder CA, Raman AV, Girguis PR, Levin LA, Knoll AH (2013) Oxygen, ecology, and the Cambrian radiation of animals. Proc Natl Acad Sci 110:13446–13451

Steiner M, Wallis E, Erdtmann BD, Zhao YL, Yang RD (2001) Submarine-hydrothermal exhalative ore layers in black shales from South China and associated fossils - insights into a Lower Cambrian facies and bio-evolution. Palaeogeogr Palaeoclimatol Palaeoecol 169:165–191

Stylo M, Neubert N, Wang Y, Monga N, Romaniello SJ, Weyer S, Bernier-Latmani R (2015) Uranium isotopes fingerprint biotic reduction. Proc Natl Acad Sci 112:5619–5624

Taylor SR, McLennan SM (1995) The geochemical evolution of the continental crust. Rev Geophys 33:241–265

Tissot FLH, Dauphas N (2015) Uranium isotopic compositions of the crust and ocean: age correlations, U budget and global extent of modern anoxia. Geochim Cosmochim Acta 167:113–143

Tossell JA (2005) Calculating the partitioning of the isotopes of Mo between oxidic and sulfidic species in aqueous solution. Geochim Cosmochim Acta 69:2981–2993

Voegelin AR, Pettke T, Greber ND, von Niederhäusern B, Nägler TF (2014) Magma differentiation fractionates Mo isotope ratios: evidence from the Kos Plateau Tuff (Aegean Arc). Lithos 190-191:440–448

Wang X, Johnson TM, Lundstrom CC (2015) Low temperature equilibrium isotope fractionation and isotope exchange kinetics between U(IV) and U(VI). Geochim Cosmochim Acta 158:262–275

Wasylenki LE, Rolfe BA, Weeks CL, Spiro TG, Anbar AD (2008) Experimental investigation of the effects of temperature and ionic strength on Mo isotope fractionation during adsorption to manganese oxides. Geochim Cosmochim Acta 72:5997–6005

Wen HJ, Carignan J (2011) Selenium isotopes trace the source and redox processes in the black shale-hosted Se-rich deposits in China. Geochim Cosmochim Acta 75:1411–1427

Wen HJ, Carignan J, Cloquet C, Zhu XK, Zhang YX (2010) Isotopic delta values of molybdenum standard reference and prepared solutions measured by MC-ICP-MS: proposition for delta zero and secondary references. J Anal At Spectrom 25:716–721

Wen HJ, Fan HF, Zhang YX, Cloquet C, Carignan J (2015) Reconstruction of early Cambrian ocean chemistry from Mo isotopes. Geochim Cosmochim Acta 164:1–16

Weyer S, Anbar AD, Gerdes A, Gordon GW, Algeo TJ, Boyle EA (2008) Natural fractionation of $^{238}U/^{235}U$. Geochim Cosmochim Acta 72:345–359

Wille M, Nägler TF, Lehmann B, Schröder S, Kramers JD (2008) Hydrogen sulphide release to surface waters at the Precambrian/Cambrian boundary. Nature 453:767–769

Wu S, Zhao YH, Feng XB, Wittmeier A (1996) Application of inductively coupled plasma mass spectrometry for total metal determination in silicon-containing solid samples using the microwave-assisted nitric acid hydrofluoric acid hydrogen peroxide boric acid digestion system. J Anal At Spectrom 11:287–296

Wu T, Yang RD, Gao JB, Li J (2021) Age of the Lower Cambrian vanadium deposit, east Guizhou, South China: evidences from age of tuff and carbon isotope analysis along the Bagong section. Open Geosci 13:999–1012

Xu LG, Lehmann B, Mao J, Qu WJ, Du AD (2011) Re-Os age of polymetallic Ni-Mo-PGE-Au mineralization in Early Cambrian black shales of South China – a reassessment. Econ Geol 106:511–522

Xu LG, Lehmann B, Mao JW (2013) Seawater contribution to polymetallic Ni-Mo-PGE-Au mineralization in Early Cambrian black shales of South China: evidence from Mo isotope, PGE, trace element, and REE geochemistry. Ore Geol Rev 52:66–84

Xu LG, Lehmann B, Mao JW, Nägler TF, Neubert N, Böttcher M, Escher P (2012) Mo isotope and trace element patterns of Lower Cambrian black shales in South China: multi-proxy constraints on the paleoenvironment. Chem Geol 318-319:45–59

Xu LG, Mao JW (2021) Trace element and C-S-Fe geochemistry of Early Cambrian black shales and associated polymetallic Ni-Mo sulfide and vanadium mineralization, South China: implications for paleoceanic redox variation. Ore Geol Rev 135:104210

Yin RS, Xu LG, Lehmann B, Lepak RF, Hurley JP, Mao JW, Feng XB, Hu RZ (2017) Anomalous mercury enrichment in Early Cambrian black shales of South China: mercury isotopes indicate a seawater source. Chem Geol 467:159–167

Zhang YX, Wen HJ, Fan HF (2009) Chemical pretreatment methods for measurement of Mo isotope ratio on geological samples. Chin J Anal Chem 37:216–220

Zhu MY, Zhang JM, Steiner M, Yang AH, Li GX, Erdtmann BD (2003) Sinian-Cambrian stratigraphic framework for shallow- to deep-water environments of the Yangtze Platform: an integrated approach. Prog Nat Sci 13:951–960